

ARTICLE

Open Access

Neuromodulation of BAG co-chaperones by HIV-1 viral proteins and H₂O₂: implications for HIV-associated neurological disorders

Michael R. Duggan^{1,2}, Taha Mohseni Ahooyi¹, Vinay Parikh² and Kamel Khalili¹

Abstract

Despite increasing numbers of aged individuals living with HIV, the mechanisms underlying HIV-associated neurological disorders (HANDs) remain elusive. As HIV-1 pathogenesis and aging are characterized by oxidative stress as well as altered protein quality control (PQC), reactive oxygen species (ROS) themselves might constitute a molecular mediator of neuronal PQC by modulating BCL-2 associated athanogene (BAG) family members. Present results reveal H₂O₂ replicated and exacerbated a reduction in neuronal BAG3 induced by the expression of HIV-1 viral proteins (i.e., Tat and Nef), while also causing an upregulation of BAG1. Such a reciprocal regulation of BAG3 and BAG1 levels was also indicated in two animal models of HIV, the doxycycline-inducible Tat (iTat) and the Tg26 mouse. Inhibiting oxidative stress via antioxidants in primary culture was capable of partially preserving neuronal BAG3 levels as well as electrophysiological functioning otherwise altered by HIV-1 viral proteins. Current findings indicate HIV-1 viral proteins and H₂O₂ may mediate neuronal PQC by exerting synergistic effects on complementary BAG family members, and suggest novel therapeutic targets for the aging HIV-1 population.

Introduction

Amongst persons living with HIV, the implementation of combined antiretroviral therapies (cARTs) since the mid-1990s has significantly increased life expectancies and decreased mortality rates such that approximately half of the HIV+ population is now ≥ 50 years of age¹. However, this cohort is consistently found to be at a significantly greater risk for developing HIV-associated neurological disorders (HANDs), a spectrum of cognitive deficits reflecting impairments across several domains (e.g., executive functioning, memory, attention) and ensuing detriments on daily functioning^{2–6}. Furthermore, despite the active debate surrounding the prevalence of HAND, it is evident HIV-infected individuals in the cART

era illustrate significantly greater risk for the development and progression of neurocognitive deficits compared to the general population^{7,8}. Thus, examining the neurobiological underpinnings of HAND appear warranted, including the potential consequences of HIV protein toxicity on homeostatic processes in neurons.

While its underlying mechanisms remain debated, evidence suggests the adverse effects of specific viral proteins may contribute to HAND, including the trans-activator of transcription (Tat) and the negative factor (Nef) proteins^{9,10}. Tat can compromise a variety of homeostatic processes in the CNS, including neuronal viability, synapse formation, and neuroinflammatory profiles^{11–13}. Furthermore, the consequences of Tat on cellular homeostasis may be due to its capacity to significantly increase levels of oxidative stress^{14–17}. In addition, Nef may promote neuronal dysfunction through several complementary processes in the brain, including impaired metabolic activity, elevated neuronal cell death, and increased levels of neuroinflammation^{18–21}. Consistent with the effect of Tat,

Correspondence: Kamel Khalili (kamel.khalili@temple.edu)

¹Department of Neuroscience, Center for Neurovirology, Lewis Katz School of Medicine at Temple University, 3500 N. Broad Street, 7th Floor, Philadelphia, PA 19140, USA

²Department of Psychology, College of Liberal Arts at Temple University, 1701 N 13th Street, 9th Floor, Philadelphia, PA 19122, USA

Edited by Joern Steinert

© The Author(s) 2021



Open Access This article is licensed under a Creative Commons Attribution 4.0 International License, which permits use, sharing, adaptation, distribution and reproduction in any medium or format, as long as you give appropriate credit to the original author(s) and the source, provide a link to the Creative Commons license, and indicate if changes were made. The images or other third party material in this article are included in the article's Creative Commons license, unless indicated otherwise in a credit line to the material. If material is not included in the article's Creative Commons license and your intended use is not permitted by statutory regulation or exceeds the permitted use, you will need to obtain permission directly from the copyright holder. To view a copy of this license, visit <http://creativecommons.org/licenses/by/4.0/>.

elevations in oxidative stress are observed in response to Nef^{22–24}. Moreover, these viral proteins may precipitate such increases in part by altering mitochondrial dynamics of neurons²⁵.

Due to abnormal levels of reactive oxygen species (ROS), oxidative stress can induce variation in numerous homeostatic mechanisms that are associated with compromised neuronal functioning and neurodegenerative diseases²⁶. H₂O₂ is particularly unique given its lack of an unpaired electron, which allows it to be more abundant and maintain the longest half-life compared to other ROS, in addition to its capacity to permeate lipid bilayers²⁷. While increased measures of oxidative stress are commonly observed in the CNS of HIV-1 infected individuals, accumulating evidence suggests such elevations can compromise efficient neuronal functioning and may contribute to HAND^{28,29}. Similarly, the aging CNS is correlated with elevations in oxidative stress, and such ROS imbalances are associated with impaired neuronal functioning that is otherwise observed in age-related neurodegenerative diseases, including Alzheimer's disease^{30–32}. Thus, oxidative stress, particularly H₂O₂, could mediate the deleterious effects induced by HIV-1 viral proteins in the aging brain.

Along with abnormal ROS, both HIV infection and aging are associated with alterations in neuronal protein quality control (PQC)^{33–35}. Through their shared BAG domain, the BCL-2 associated athanogene (BAG) family of co-chaperones are necessary for efficient PQC by functioning as nucleotide exchange factors, thereby modulating the activity of Hsp70 via its ATPase domain^{36,37}. BAG3, in addition to stimulating removal of malformed or aggregated polypeptides via autophagy, is emerging as a crucial regulator of stress granules (SGs), membrane-less compartments that can facilitate aberrant accumulation of aggregated proteins^{38,39}. Along with its potent anti-apoptotic properties, growing data also suggest BAG1 levels are inversely proportional to BAG3, potentially due to its complementary clearance of substrates via the ubiquitin proteasomal system (UPS)^{40–42}. Such a functional transition between BAG3 and BAG1 dependent PQC is postulated to be an adaptive preservation of neuronal homeostasis under conditions that might otherwise facilitate neuropathogenesis, such as viral infection, aging, and elevated oxidative stress^{43,44}. Therefore, in response to HIV-1 viral proteins or aging, H₂O₂ itself could constitute an important modulator of neuronal PQC by regulating BAG family members.

Consistent with this hypothesis, recent reports suggest variation in certain BAG family members can be induced by HIV-1 Tat, as well as aging and ROS conditions^{42,45,46}. Investigations from our laboratory have demonstrated that a significant downregulation of BAG3 is characteristic of

HIV-transgenic mouse models as well as primary rat neurons expressing the Tat protein⁴⁶. Furthermore, an inverse relationship between BAG3 and BAG1 levels has been reported in cell lines exposed to H₂O₂, in multiple brain regions of aged mice, as well as hippocampal slices from aged rats^{42,45}. However, it remains unclear how elevations in H₂O₂ may directly modulate BAG family members in primary neurons, particularly in comparison to HIV-1 proteins.

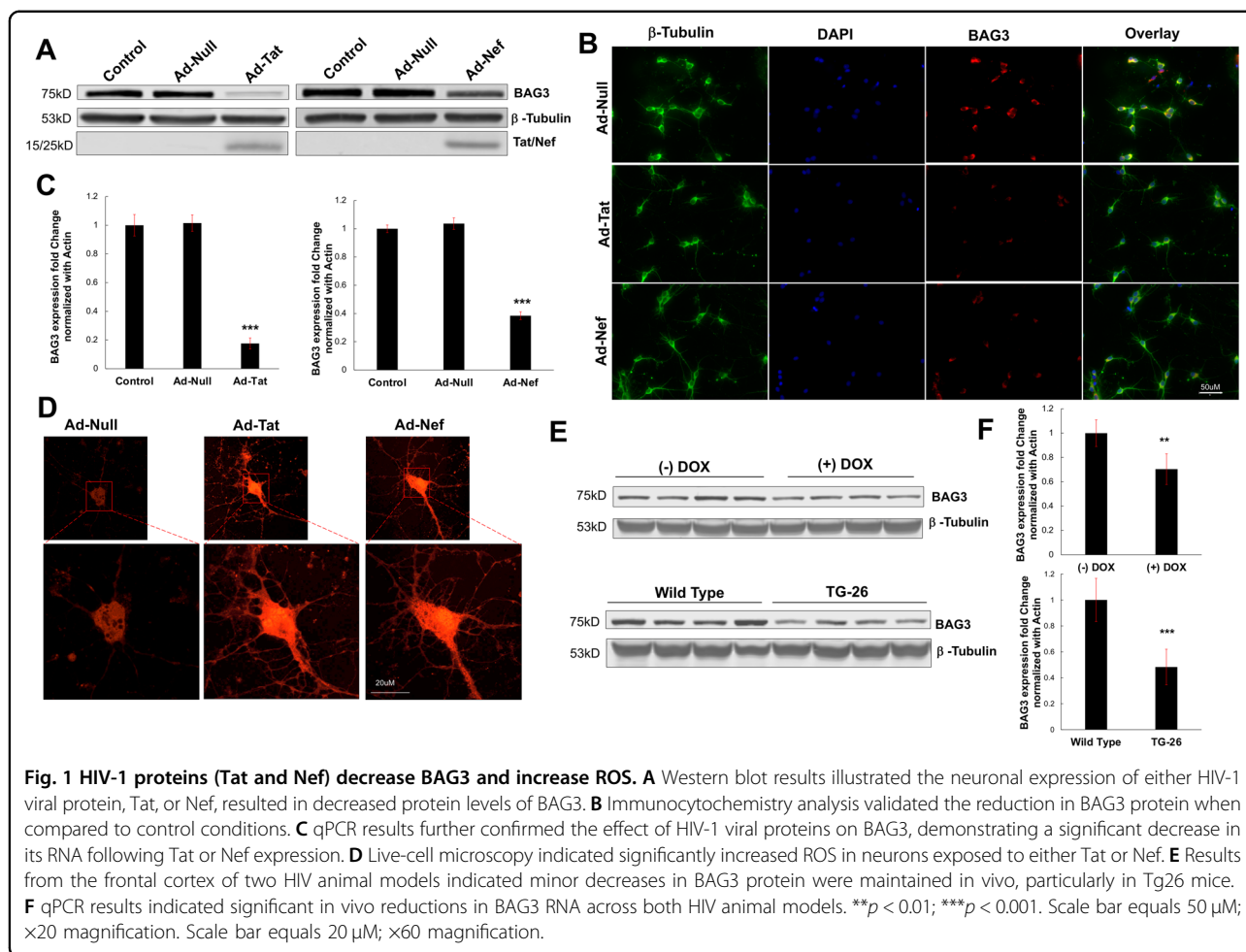
To address this aim, the current experiments interrogate the effects of viral proteins Tat and Nef as well as H₂O₂ in primary neurons cultured from rat embryos. Findings reveal a reduction in neuronal BAG3 induced by the expression of HIV-1 viral proteins (i.e., Tat and Nef) was emulated and exacerbated by H₂O₂, which also caused an upregulation of BAG1. Inhibiting oxidative stress via antioxidants in primary culture was capable of partially preserving neuronal BAG3 levels as well as electrophysiological functioning otherwise altered by HIV-1 viral proteins. Therefore, the current study provides mechanistic insights relevant to treatment development for our aging HIV-1 population.

Results

HIV-1 viral proteins (Tat and Nef) decrease BAG3 and increase ROS

Primary neurons expressing HIV-1 Tat displayed significantly reduced levels of BAG3, consistent with previous observations from our laboratory⁴⁶. Immunoblotting and fluorescent microscopy data demonstrated a significant decrease in BAG3 protein in response to Tat (Fig. 1A, B; Supplementary Fig. 1A, B). Similarly, we found the expression of HIV-1 Nef in primary neurons significantly attenuated BAG3 protein (Fig. 1A, B; Supplementary Fig. 1A, B). Moreover, both Tat and Nef were capable of independently downregulating BAG3 RNA (Fig. 1C). In assessing variations in oxidative stress due to such viral proteins, live-cell confocal microscopy illustrated significant elevations ROS following the expression of Tat or Nef (Fig. 1D; Supplementary Fig. 1C).

To determine if the pattern of BAG3 downregulation associated with viral proteins is maintained in vivo, cortical tissue from two distinct HIV animal models (iTat and Tg26) was analyzed. In a doxycycline-inducible mouse model (iTat), decreases in BAG3 protein and RNA were detected in response to Tat (Fig. 1E; Supplementary Fig. 1D). In Tg26-HIV mice, which express multiple viral proteins including Tat and Nef, more abundant significant reductions in BAG3 levels were observed (Fig. 1E, F; Supplementary Fig. 1D). Together, initial findings indicate the viral proteins Tat and Nef are capable of inducing oxidative stress in neurons, while concomitantly mitigating BAG3 levels.



H₂O₂ treatment conditions

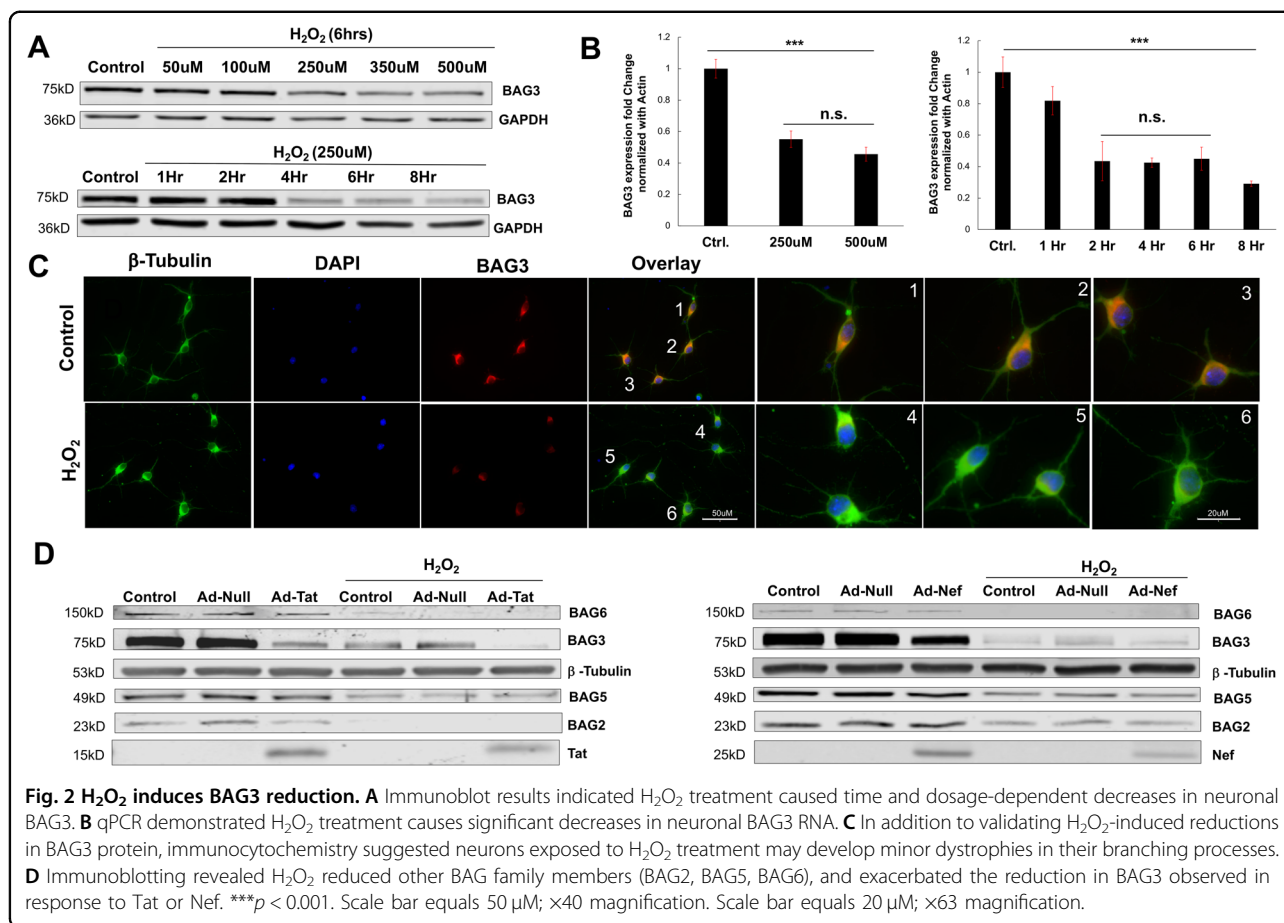
Next, we sought to examine if oxidative stress via H₂O₂ was capable of regulating neuronal BAG family members independent of HIV-1 viral protein expression. However, the optimal treatment parameters for H₂O₂ in primary neuronal culture are not well-established, due to the lack of studies employing H₂O₂ in primary neuronal cultures as well as the reliability of techniques used to assess its kinetics^{47–50}. Based on the conditions and techniques available in the limited literature, several experiments were initially conducted to determine the parameters of H₂O₂ that alter general metabolic activity without compromising viability.

At a fixed duration of 6 h, H₂O₂ significantly decreased metabolic activity at dosages above 150 μM as indicated by MTT assay, while trypan blue staining suggested cell viability was significantly mitigated at concentrations above 250 μM (Supplementary Fig. 2A, B). Utilizing a 250 μM concentration, time-course experiments illustrated significantly decreased metabolism between 2 and 6 h of treatment, while significant increased cell death was observed after 8 h of treatment (Supplementary

Fig. 2C, D). Therefore, such fixed parameters (i.e., 250 μM , 6 h) were selected as the optimal treatment conditions in succeeding experiments.

H₂O₂ induces BAG3 reduction

In primary neurons exposed to H₂O₂, significant reductions in BAG3 were observed. Dosage experiments revealed concentrations of 250 μM and above significantly decreased BAG3 protein and RNA (Fig. 2A, B). While using this fixed dosage, time-course experiments illustrated such decreases in BAG3 protein were evident at approximately 4 h post-treatment, while significant reductions in RNA precede this reduction by ~ 2 h (Fig. 2A, B). Fluorescent microscopy validated such significant reductions in BAG3 following treatment of 250 μM for 6 h; furthermore, this illuminated morphological alterations in neurons exposed to H₂O₂, with some of these cells developing dystrophy in their processes compared to control conditions (Fig. 2C; Supplementary Fig. 3A). Interestingly, treatment of primary neurons with moderate dosages (100 μM) for extended durations (6–8 h) emulated these declines in BAG3 protein, while minimal dosages (50 μM)



were unsuccessful in perturbing BAG3 protein levels at any time point (Supplementary Fig. 3B).

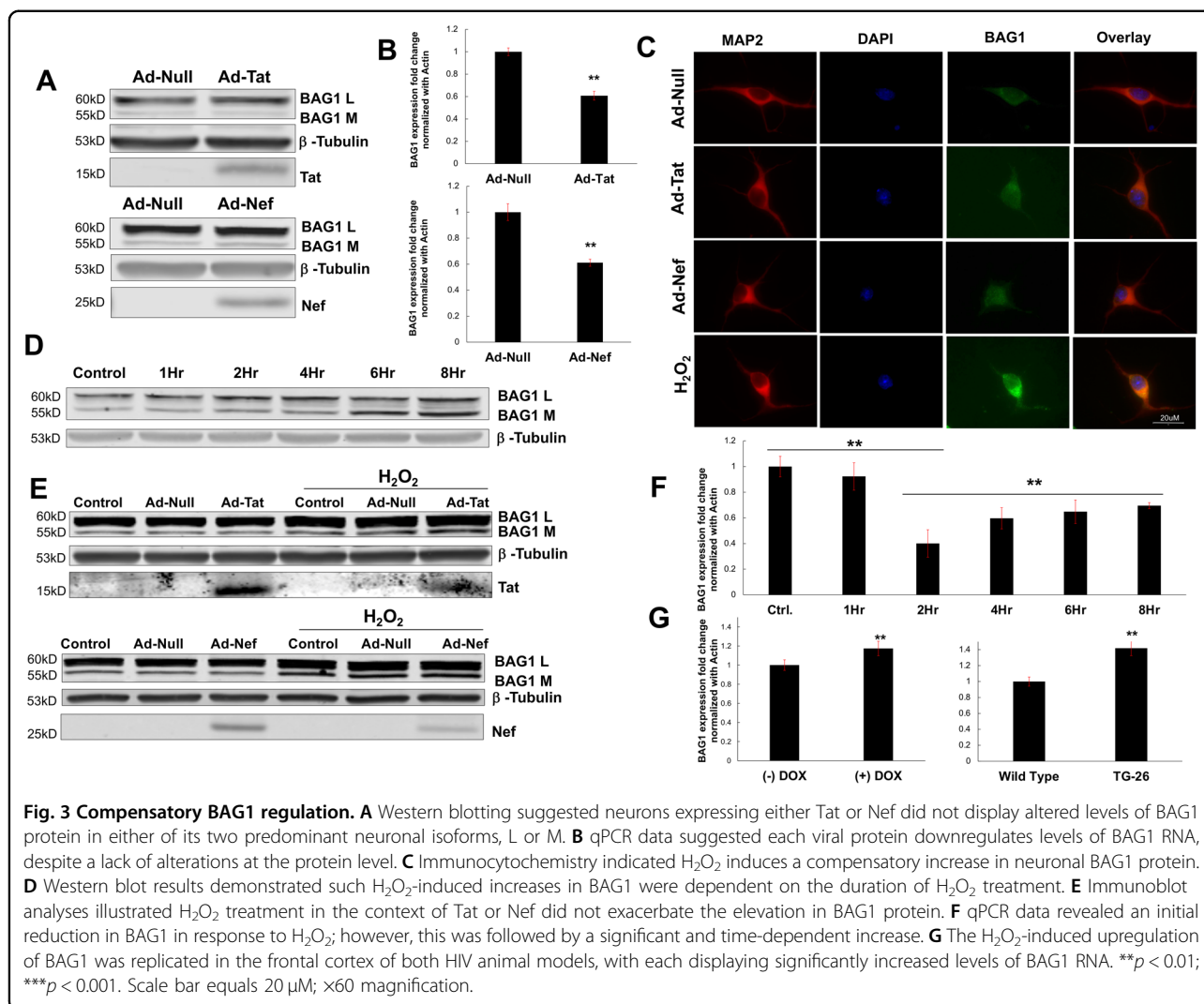
Strikingly, the combination of H₂O₂ and either viral protein Tat or Nef resulted in an additive effect, exacerbating the reduction in BAG3 (Fig. 2D). Such an additive effect was not observed when primary neurons co-expressed both viral proteins (Supplementary Fig. 3C). Moreover, decreases in BAG3 appeared to be neuronal-specific, provided that primary rat astrocytes failed to show similar sensitivity to H₂O₂ treatment (Supplementary Fig. 3D). In addition to BAG3, immunoblotting analysis also suggested H₂O₂ treatment reduced the protein levels of several other BAG family members, namely BAG6, BAG5, and BAG2 (Fig. 2D). Together, these data revealed the capacity of H₂O₂ to directly alter levels of BAG family members in both the transcription and translation levels, particularly BAG3, and support the postulation that oxidative stress is an important regulator of neuronal BAG proteins.

Compensatory BAG1 regulation

Given their complimentary roles in autophagy (i.e., BAG3) and proteasomal degradation (i.e., BAG1), we next determined whether a downregulation in BAG3 was

associated with a compensatory upregulation of BAG1^{51,52}. In primary neurons expressing either Tat or Nef, no significant variation in BAG1 protein was observed, either by immunoblot or fluorescent microscopy (Fig. 3A, C). Variation in BAG1 protein reflected its predominant rat neuronal isoforms, L and M, consistent with previous observations in BAG1 protein levels and calculated molecular weights⁵³. However, significant reductions in BAG1 RNA were found in response to either viral protein (Fig. 3B). Differences in BAG1 RNA reflected both its predominant rat neuronal isoforms⁵⁴.

In contrast, cells exposed to H₂O₂ displayed significantly elevated levels of BAG1. Immunocytochemistry indicated increases in BAG1 protein levels following 6 h of H₂O₂ treatment, while immunoblot results indicated this increase was dependent on the duration of treatment (Fig. 3C, D; Supplementary Fig. 4A). Moderate H₂O₂ dosages (100 μM) and minimal dosages (50 μM) were unsuccessful in perturbing BAG1 protein levels (Supplementary Fig. 4B). Taken together, these results are consistent with the time-dependent decreases in BAG3 found in previous experiments and suggest a decrease in BAG3 may precede the increase in BAG1 levels. However, unlike the additive effect on BAG3, the



combination of H_2O_2 with Tat or Nef did not exacerbate the increase in BAG1 (Fig. 3E; Supplementary Fig. 4C).

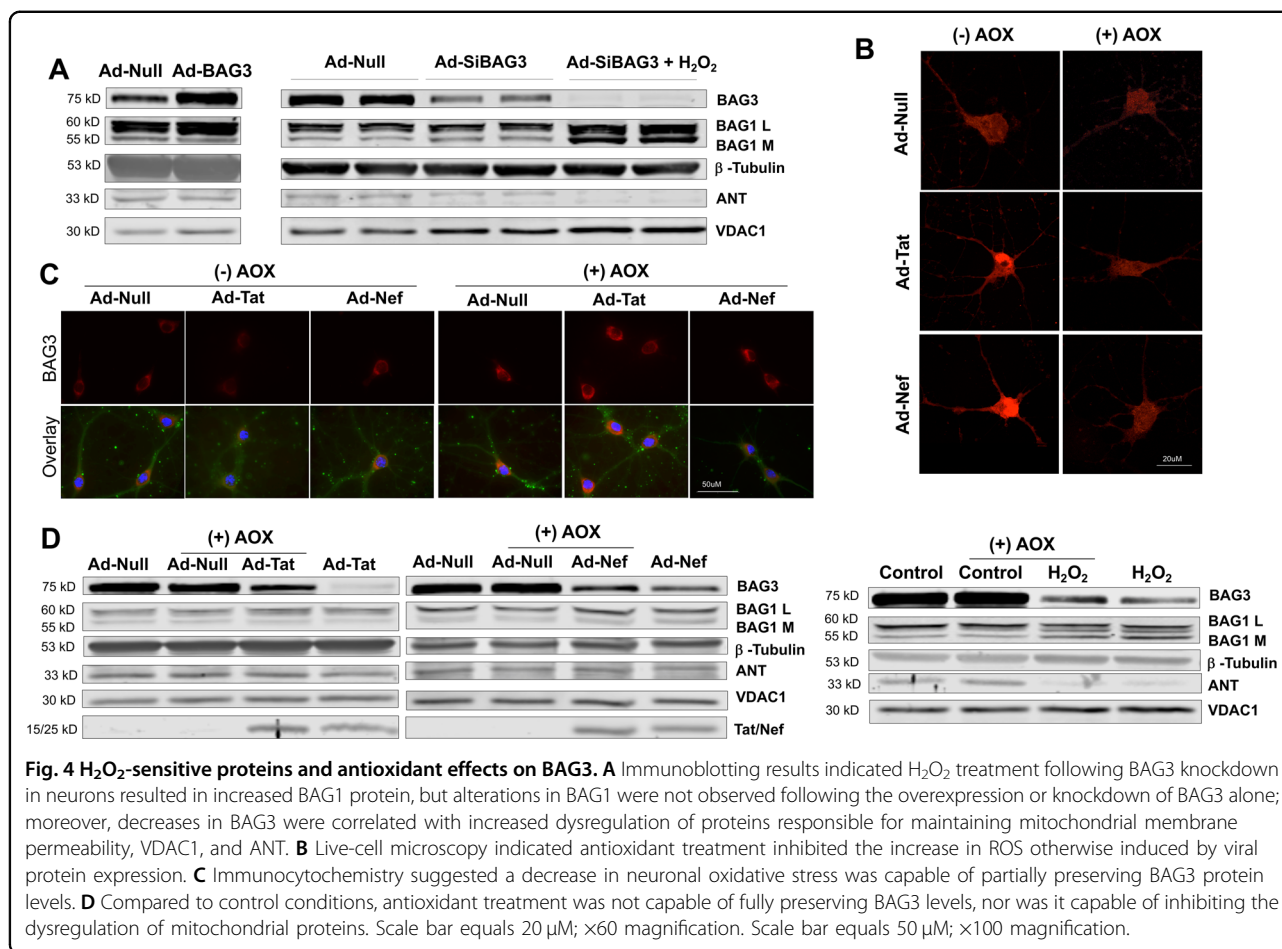
Consistent with the downregulation induced by HIV-1 viral proteins (i.e., Fig. 3B), neurons exposed to H_2O_2 initially displayed significant decreases in BAG1 RNA, most notably following 2 h of treatment; however, H_2O_2 also triggered a significant increase in BAG1 RNA after this initial decrease, although levels did not completely return to baseline (Fig. 3F). Such an inverse regulation of BAG1, compared to BAG3, was also observed in each animal model, with iTat and Tg26-HIV mice displaying significantly increased measures of BAG1 RNA compared to controls (Fig. 3G).

H_2O_2 -sensitive proteins and antioxidant effects on BAG3

Additional data indicated the dynamic effects on neuronal BAG1 and BAG3 due to H_2O_2 was associated with alterations in several mitochondrial proteins as well as polypeptides known to interact with BAG family

members. Primary neurons treated with H_2O_2 following BAG3 knockdown displayed a substantial BAG1 upregulation, while significant alterations in BAG1 were not observed following the overexpression or knockdown of BAG3 alone (Fig. 4A; Supplementary Fig. 5A). These decreases in BAG3 were associated with increased dysregulation of proteins responsible for maintaining mitochondrial membrane permeability; here, decreases in ANT and increases in VDAC1 following BAG3 knockdown were exacerbated by H_2O_2 (Fig. 4A; Supplementary Fig. 5B). In addition, neurons exposed to H_2O_2 maintained alterations in several other proteins known to bind with and influence BAG family member functioning, including Bcl-2, LC3, and Hsc/Hsp 70 (Supplementary Fig. 5C).

The direct inhibition of oxidative stress in neurons was capable of partially preserving BAG3 levels. Initial experiments employing live-cell microscopy confirmed the application of antioxidants (AOX) was capable of inhibiting



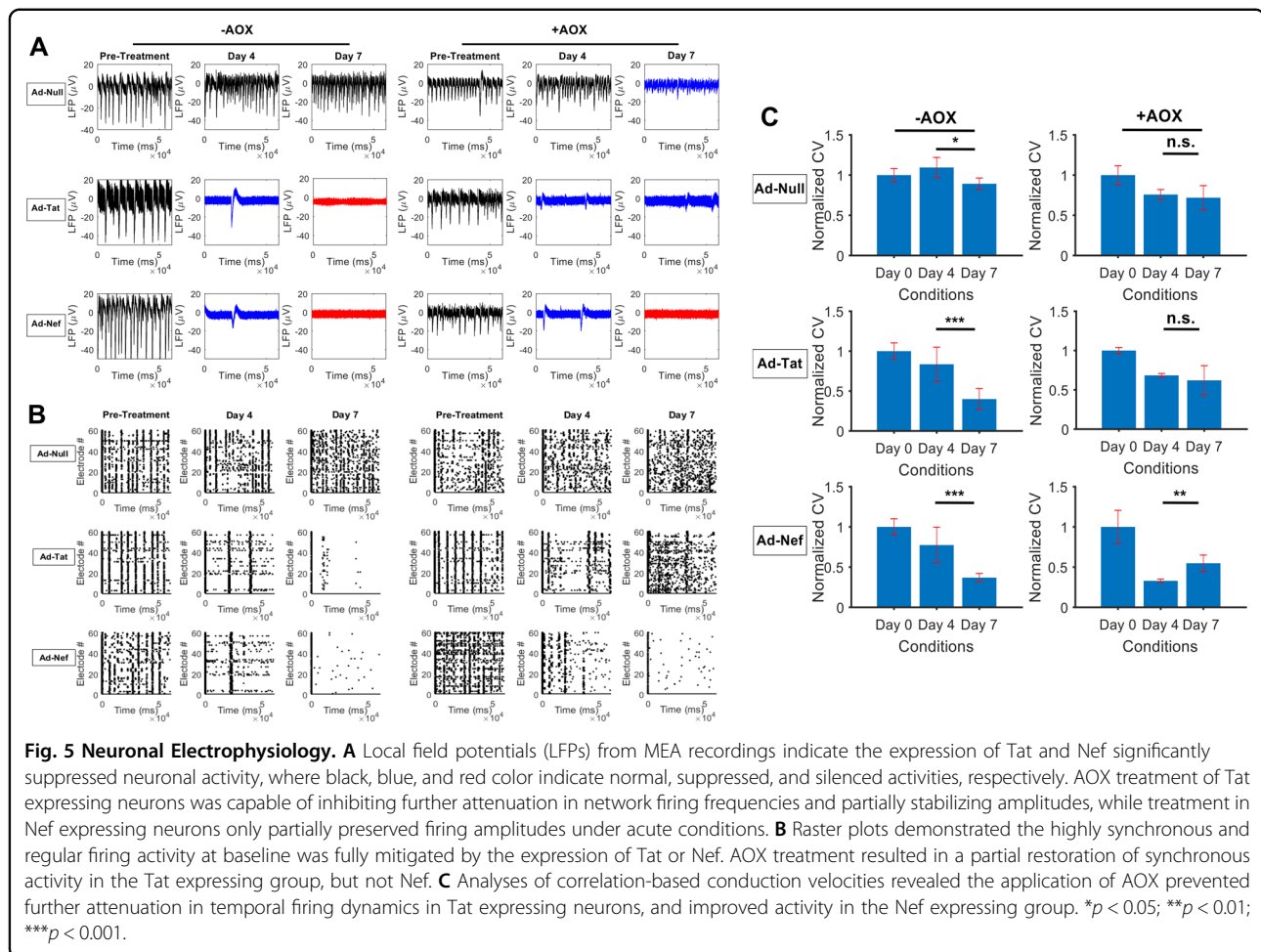
the increase in ROS otherwise induced by viral protein expression (Fig. 4B; Supplementary Fig. 5D). Due to cross-reactivity between MitoSOX reagents with H₂O₂ in solution, we were unable to reliably discern if direct application of H₂O₂ was ameliorated by AOX. While immunoblotting and fluorescent microscopy confirmed AOX partially preserved BAG3 protein levels otherwise reduced by HIV-1 viral proteins, results suggested AOX treatment was not capable of mitigating the dysregulation induced by H₂O₂ (i.e., alterations in BAG3, BAG1, and mitochondrial proteins) (Fig. 4C, D; Supplementary Fig. 6A–C).

Neuronal electrophysiology

Assessment of electrophysiological measurements indicated AOX was capable of partially preserving neuronal functioning otherwise dysregulated by HIV-1 viral proteins, particularly Tat (Fig. 5A; Supplementary Fig. 7A). As shown by LFP signals and quantifications, Tat and Nef suppressed neuronal activity in terms of amplitude and spiking frequency compared with Ad-Null treated controls. This behavior continued to develop leading to complete attenuation of neuronal activity under Tat and Nef expression. Surprisingly, AOX treatment of Tat

expressing neurons was capable of preserving activity measures by inhibiting further attenuation in network firing frequencies and partially stabilizing amplitudes. While AOX treatment of Nef expressing neurons partially preserved firing amplitudes under acute conditions, it was incapable of inhibiting long-term attenuation in amplitudes or preserving firing frequencies at any time point.

In evaluating synchronous and spontaneous activity of neuronal populations, analysis of baseline measurements illustrated regular bursting activity in all MEAs (Fig. 5B). In the absence of AOX treatment, neurons transduced with Ad-Tat or Ad-Nef consistently displayed disrupted firing patterns across electrodes. Treating neurons with AOX resulted in a partial restoration of synchronous activity in the Tat expressing group, but not Nef. Analyses of conduction velocities quantified the speed at which similar patterns of activity propagated across MEAs, whether in the form of spikes or subthreshold oscillations (Fig. 5C). In agreement with the measures above, data indicated suppressed conduction velocities in neuronal cultures expressing Tat or Nef compared to negative controls. Interestingly, the application of AOX prevented further attenuation in activity patterns amongst Tat



expressing neurons, and improved activity in the Nef expressing group. Further analyses of frequency content as well as synchronous activity within clusters of neurons indicated minimal benefits upon AOX treatment, and confirmed the adverse effects of Tat and Nef (Supplementary Fig. 7B, C). Notably, the effects of AOX under H_2O_2 conditions could not be reliably examined due to peroxide-induced electrical interference during recording sessions.

Discussion

The current findings address the potential for HIV-1 viral proteins and H_2O_2 to induce variation in neuronal BAG family members, a family of proteins responsible for efficient PQC. Both Tat and Nef viral proteins facilitated elevations in intraneuronal ROS and decreased BAG3 levels, while also disrupting neuronal firing activity. H_2O_2 exacerbated the reduction in BAG3 and induced an upregulation of BAG1. Such inverse ratios were maintained in two animal models which express viral proteins in the CNS, the doxycycline-inducible Tat (iTat) and Tg26 mouse. Interestingly, the inhibition of oxidative

stress in primary neurons was capable of partially preserving electrophysiological functioning and BAG3 levels otherwise altered by HIV-1 viral proteins. Results support the role of H_2O_2 as a modulator of neuronal PQC by regulating BAG family members in response to HIV-1 viral proteins or other potential sources of oxidative stress, such as aging (Supplementary Fig. 8).

The pattern of BAG3 and BAG1 regulation reported herein warrants consideration and emphasizes the implications of cell-specific experimental paradigms. As oxidative stress and aging can mitigate proteasome functioning while also increasing concentrations of aggregate-prone polypeptides, a compensatory yet disproportionate demand for BAG3 over BAG1 has been hypothesized in response to perturbation in neuronal homeostasis^{44,55}. Indeed, in a cell line model of aging as well as neural cell lines clonally selected for resistance to oxidative stress, a group of researchers recently reported increasing BAG3 and decreasing BAG1 in response to H_2O_2 ^{42,43,45}. This group reported similar results in aged brain samples containing both neurons and glia (i.e., tissue homogenates, ex vivo hippocampal slices)⁴². However, researchers indicated such

BAG regulation was specific to neurons (see Fig. 2F in Gamerding et al., 2009), consistent with results obtained here (see Supplementary Fig. 3D). Therefore, the direction of BAG3 and BAG1 regulation by H₂O₂ in the current experiments may be reflective of cell-specific responses obtained from primary neurons, whereas prior experimental procedures may reflect general cellular adaptations in the neural milieu. In light of accumulating evidence distinguishing the molecular biology of neurons from other cell types in the brain, particularly in response to aging and neuropathogenesis, such cell-specific responses are plausible and increasingly relevant^{56,57}.

Current experiments provided further mechanistic insights for the biomolecular underpinnings of HIV neuropathogenesis, particularly regarding the consequences of viral proteins on homeostatic functioning in neurons^{21,58}. Further investigations are necessary to validate the physiological relevance of these data in the context of recombinant Tat and Nef proteins. In addition, while we reported increased BAG1 and decreased BAG3 RNA in brain tissues of two different HIV animal models, this pattern of regulation may reflect a compensatory adaptation between neuronal and non-neuronal cells to confer neuroprotection during adulthood^{59,60}. Therefore, future studies should determine if this regulation of neuronal BAG proteins in animal models of HIV is age-dependent, given that cell-specific population densities and functioning can vary in the aging CNS, compared to adolescence or adulthood⁶¹.

Taken together, our results suggest the regulation of oxidative stress in conjunction with PQC modulators may result in novel therapeutic opportunities in HAND. Specifically, data from HIV-1 proteins indicated antioxidants could partially preserve neuronal electrophysiology and BAG3 levels. This is consistent with the otherwise adverse consequences of Tat and Nef, which include the generation of abnormal ROS and impairments in PQC^{17,29,62,63}. While the reliability of antioxidant therapeutics remains debated, some reports suggest their application in combination with other treatments can result in enhanced outcomes for neurodegenerative conditions, including AD^{64,65}. As the selective augmentation of BAG proteins has proved efficacious in the context of other age-related neurological diseases, targeted PQC therapies in combination with antioxidant therapies may provide novel treatments amongst our aging HIV population^{66–69}.

Materials and methods

Primary neuronal culture and cell treatment

Tissue preparation and cell cultures were performed according to Temple University's Institutional Animal Care and Use Committee and the National Institute of Health (NIH) guidelines. As described previously, primary neuronal cultures were prepared using dissected E18

prenatal rat embryonic brains^{46,70}. After digestion in trypsin solution (0.25%), neurons were plated on tissue culture plates, slides, or microelectrode arrays, MEAs (see below), that were coated with poly-D-lysine (Sigma-Aldrich, St. Louis, MO) as well as laminin (Invitrogen 23017, USA). Cells were maintained 17 days (25 days for MEA studies) in vitro (DIV) prior to treatments, at which point cells were randomly assigned to conditions and experiments were initiated. All experiments were completed in triplicate to confirm the reliability of results and to obtain appropriate power for statistical analyses.

To ensure no degradation of reagents, H₂O₂ treatments proceeded using indicated dilutions prepared from stock immediately prior to their application (VWR BDH7690, USA); solutions were prepared under sterile conditions with diH₂O (100 μ L total volume). Neurons were transduced with Ad-Null (Vector Biolabs, Malvern, PA), Ad-Tat (made in-house), Ad-Nef (made in-house), Ad-siBAG3 (Vector Biolabs, Malvern, PA), and Ad-BAG3 (Vector Biolabs, Malvern, PA). To produce viral constructs in-house for transduction, cDNA was cloned from HIV strain 89.6 into compatible restriction sites of the shuttle plasmid pDC515(IO) and subsequently rescued by co-transfection with pBHGfrtDeltaE1,E3FLP in 293 IQ cells (Microbix Corporation, Mississauga, Ontario, Canada). The Ad was then plaque purified, amplified, and subsequently purified on cesium chloride (CsCl) gradient centrifugation. Plaque purified virus was dialyzed against elevated salt and MgCl₂ for further purification, provided that CsCl does not generate entirely pure preparations. Collected viral particles were diluted for concentration measurement at OD₂₆₀, while the virus concentration was calculated based on number of particles/ml. MOI was maintained at 1 for all vectors throughout procedures. Transduction durations were maintained in accordance with previous experiments in our laboratory (72 h). To assess the combined effect of H₂O₂ with viral proteins, H₂O₂ treatments were initiated after the transduction period; this time point remained consistent for all H₂O₂ experiments. Antioxidant (AOX) treatments were applied in a manner previously described^{71,72}; here, a proprietary antioxidant solution at recommended dilutions (1:1000 in culture media; 100 μ L total volume) was applied in culture for 24 h following transduction (A1345; Sigma-Aldrich, St. Louis, MO).

Animal models

Animal procedures and protocols were performed according to Temple University's Institutional Animal Care and Use Committee and the National Institute of Health (NIH) guidelines. Adult male mice (18–28 g) were singly housed in a temperature (21–23°) and humidity-controlled vivarium with constant airflow on a reverse 12-h light/dark cycle (lights on/off at 09:00 EST). Food and water were available ad libitum. Two mouse models

previously in our laboratory were utilized in the present experiments. Tg26-HIV-transgenic mice are a widely used and well-described mouse model that encode the entire pNL4–3 HIV-1 genome, except a segment of gag/pol genes. This model expresses HIV viral proteins such as Tat and Nef, while exhibiting neuropathology observed upon HIV infection, including neurocognitive deficits. Doxycycline (DOX)-inducible GFAP promoter-driven HIV-1 Tat transgenic mice were provided by the Comprehensive NeuroAIDS Center. This model conditionally-expresses the HIV-1 Tat_{1–86} protein in an astrocyte-specific manner under the control of a GFAP-driven Tet-on promoter, which is activated in the presence of DOX. Both iTat and their control littermates were randomly selected to receive doxycycline hyclate (DOX) orally over the course of 6 weeks (S3888; Bioserv, Flemington, NJ). C57BL/6J mice maintained in our laboratory's colony were utilized as controls. All mice in each group ($n = 4$) were euthanized at similar time points (~6 months old) and brain tissue was harvested for subsequent analyses. As many of the cognitive deficits manifested in HAND patients during the post-cART era are associated with aberrant functioning in cortical regions of the brain (e.g., attention, executive functions, learning), analyses focused on tissue from this area⁷³.

Metabolic and viability assays

To assess general metabolic activity, the MTT (3-(4,5-dimethylthiazol-2-yl)-2,5-dihydroxybenzimidazolium bromide) assay was used. Following treatment, primary rat neurons were incubated for 2 h at 37 °C in solution containing MTT according to the manufacturer's recommendations (CT015; Sigma-Aldrich, St. Louis, MO). Measures from each sample were determined as the difference between 595 and 620 nm wavelength values obtained by spectrophotometry. To gauge neuronal cell death, the trypan blue exclusion procedure was used. Here, cell solutions were prepared by equal dilution with trypan blue dye (15250061; ThermoFisher, Waltham, MA) followed by quantification using disposable slides (C10228; ThermoFisher, Waltham, MA) and an automated cell counter (AMQAF1000; ThermoFisher, Waltham, MA).

Western blotting

For immunoblotting experiments, neuronal and mouse brain samples (frontal cortex) were homogenized and lysed with RIPA buffer (25 mM Trizma base pH 7.6, 150 mM NaCl, 1% NP-40, 1% sodium deoxycholate, 0.1% SDS) containing a protease inhibitor cocktail (Sigma-Aldrich, St. Louis, MO). Protein concentrations were assessed by means of a standardized Bradford assay (Bio-Rad, Hercules, CA). SDS-polyacrylamide gels, 10–12%, and nitrocellulose membranes (LI-COR, Inc., Lincoln, NE) were used for electrophoretic protein separation and

transfer, respectively. To reduce non-specific binding and background, membranes were blocked in Odyssey (LI-COR) blocking buffer (1 h, room temperature). Primary (1:1000, overnight, 4 °C) and secondary (1:10,000, 1 h, room temperature) antibodies were applied followed by imaging on the Odyssey CLx Imaging System (LI-COR). Protein levels were assessed and standardized to appropriate loading controls by means of optical density analysis using Image Studio acquisition software. The following primary antibodies were used: ANT (Santa Cruz; SC11433), β -Tubulin (Sigma; T8578), Bcl-2 (Santa Cruz; SC7382), BAG1 (Santa Cruz; SC939), BAG2 (Novus Biologicals; NBP159086), BAG3 (Proteintech; 105991AP), BAG5 (Proteintech; 266281AP), BAG 6 (R&D Systems; AF6438), BAX (Santa Cruz; SC493), GAPDH (Santa Cruz; SC32233), Hsc/Hsp 70 (Santa Cruz; SC24), LC3 (Santa Cruz; L8918), Nef (Abcam; ab42355), Tat (NIH Aids Reagent Program; R705), VDAC1 (Santa Cruz; SC8017).

Immunocytochemistry

Following fixation (4% paraformaldehyde), blocking (1% BSA), and washing, neurons were labeled with the following primary antibodies (1:100, overnight, 4 °C): β Tubulin (Sigma; T8578), BAG1 (Santa Cruz; SC376848), BAG3 (Proteintech; 105991AP) MAP2 (Cell Signaling; 4542). Alexa Fluor® secondary antibodies (1:500) (ThermoFisher, Waltham, MA) and VectaShield with DAPI medium (Vector Laboratories, Burlingame, CA) were used for labeling and mounting, respectively. Imaging utilized a fluorescence microscope (BZ-X710; Keyence, Osaka, Osaka, Japan) and image processing employed the Hybrid Cell Count module within the BZ Image Analyzer software (Keyence) to obtain optical density measurements expressed in μ M per cell.

ROS quantification

To assess levels in reactive oxygen species (ROS), cells were incubated with the mitochondrial oxygen free radical indicator MitoSOX-red (Life Technologies, Carlsbad, CA) for 30 min at 37 °C. Slides were then mounted for confocal imaging in an open perfusion microincubator (PDMI-2; Harvard Apparatus) and images were obtained at 561 nm excitation by using a confocal microscope (810; Carl Zeiss, Oberkochen, Germany). Optical densitometry quantifications were expressed as fluorescence intensity normalized to areas as previously described⁷⁴.

RNA isolation and cDNA preparation

Total RNA for each neuronal and mouse brain sample (frontal cortex) was processed using the Trizol (ThermoFisher) extraction protocol followed by RNA purification using Direct-zol™ RNA MiniPrep Plus (Zymo Research, Irvine, CA) in accordance with manufacturer specifications. cDNA synthesis on total RNA samples

utilized with the High Capacity cDNA Reverse Transcription Kit (Thermo Fisher Scientific).

Real time-quantitative RT-PCR (qRT-PCR)

Sequence design for forward and reverse primers utilized the most to date reference genomes followed by submission to NCBI's Basic Local Alignment Search Tool (BLAST) to ensure the selected primers do not display similarity to other sequences. The sensitivity and specificity of primers were checked by RT-PCR using FailSafe PCR Kit (Lucigen, Middleton, WI). All qPCR reactions were conducted with the LightCycler96[®] (Roche) using the SYBR[™] Green master mix (Applied Biosystems, ThermoFisher), according to the manufacturer's specifications. Relative quantity was normalized to Actin expression. Primer sequences were as follows: Actin (Forward-5'-CAG GTCCAGACGCAGGATGGC-3'; Reverse-5'-CTACAAT GAGCTGCGTGTGGC-3'), BAG1 (Forward-5'-AGATGG TCCAGACGGAGGAA-3'; Reverse-5'-CAGATACCTC CAAGTCCTTCAGC-3'), BAG3 (Forward-5'-GGCCCTA AGGAAACTGCAT-3'; Reverse-5'-GGGAATGGGAA TGTAACCTG-3'), Tat (Forward-5'-GGAATTCACCA TGGAGCC AGTA-3'; Reverse-5'-CGGGATCCCTATT CCTTCGGGC-3').

Microelectrode array (MEA)

Neuronal activities were recorded pre-treatment (Day 0) and 96 h (Day 4) as well as 168 h (Day 7) after transduction. To ensure the assessment of AOX effects was temporally consistent with AOX effects observed in other experiments, recordings were conducted 24 h after AOX was added to half of the cultures post-transduction (i.e., 96 h). Media with or without AOX was then maintained until the final recording session on Day 7 to assess potential chronic effects of AOX treatment on neuronal functioning. In each recording session, multiple minutes of recordings were performed to acquire local field potential (LFP) of neuronal extracellular action potential at 2000 Hz (2 kHz) from 60 electrodes simultaneously. Recorded data were then transferred as numerical values in microvolts to MATLAB (Mathworks, Natick, MA) for pre- and post-processing. Low-pass filtering with cut-off frequency $f_c = 300$ Hz was applied to all recording data prior to data analysis.

LFPs of different experimental groups were visualized in MATLAB with representative channels in a 60,000 ms course (120,000 sampled points for each signal). To depict the network-wide activation and provide a measure of activity beyond a single electrode, raster plots were generated based on the time at which a spike was detected (activity exceeding three times standard deviation of the raw data) for all channels, and visualized for all time points as well as experimental groups. To show the rate at which neuronal activation travels from the source across populations, the cross-correlation values between pairs of

electrodes and their distance were used to compute conduction velocities (cm/s). These data were then normalized (nondimensionalized) with respect to initial conditions to reflect the treatment effects on wave propagation rates. For the technical details refer to ref. ⁷⁰. To examine frequency content of neuronal oscillations, time domains LFPs of all electrodes were transformed and analyzed to frequency domains using fast Fourier transform (FFT). The resulting mean and standard deviations were plotted and analyzed for each condition. To determine the effect of different experimental conditions on network-wide synchronous clusters of neurons, rank correlation matrices were first calculated across electrodes. Subsequently, hierarchical clustering identified clusters of electrodes that exhibited similar or comparable correlation patterns, number of clusters and the magnitude of correlation, which were presented in a heat map format.

Statistical analyses

Statistical procedures were optimized based on the experimental designs as well as the consistent, continuous nature of the measured variables across assays. Independent samples *t*-tests were primarily employed to compare measures between control and experimental conditions across assays. For those assays which required multiple comparisons either between or within samples, analysis of variance (ANOVA) followed by appropriate post hoc comparisons and corrections were conducted. All data were screened for normality. For MEA quantifications, mean and standard deviations of the number of detected spikes were computed across 60 electrodes for each time point and experimental group. Mean and standard deviations of maximum LFP amplitudes were also obtained for each time point/experimental group. All statistical analyses were conducted utilizing SPSS v 22 (IBM, Armonk, NY) or MATLAB (Mathworks).

Acknowledgements

The authors wish to thank past and present members of the Department of Neuroscience and Center for Neurovirology for their support, as well as sharing of ideas and reagents. This work was made possible by grant T32MH079785 and grants awarded by NIH to K.K.

Conflict of interest

The authors declare no competing interests.

Publisher's note

Springer Nature remains neutral with regard to jurisdictional claims in published maps and institutional affiliations.

Supplementary information The online version contains supplementary material available at <https://doi.org/10.1038/s41420-021-00424-0>.

Received: 29 September 2020 Revised: 4 January 2021 Accepted: 30 January 2021

Published online: 26 March 2021

References

- Hess, K. L. et al. Diagnoses of HIV infection in the United States and dependent areas, 2017. *HIV Surveill. Rep.* **29**, 17–21 (2018).
- Clifford, D. & Ances, B. HIV-associated neurocognitive disorder. *Lancet Infect. Dis.* **13**, 976–986 (2013).
- Valcour, V. et al. Higher frequency of dementia in older HIV-1 individuals: the Hawaii Aging with HIV-1 Cohort. *Neurology* **63**, 822–827 (2004).
- Chiesi, A. et al. Epidemiology of AIDS dementia complex in Europe. *AIDS* **11**, <https://doi.org/10.1097/00042560-199601010-00005> (1996).
- Janssen, R. S., Nwanyanwu, O. C., Selik, R. M. & Stehr-Green, J. K. Epidemiology of human immunodeficiency virus encephalopathy in the United States. *Neurology* **42**, 1472–1476 (1992).
- Fazeli, P. L. et al. Cognitive functioning in adults aging with HIV: a cross-sectional analysis of cognitive subtypes and influential factors. *J. Clin. Res. HIV/AIDS Prev.* **1**, 155–169 (2014).
- Schouten, J., Cinque, P., Gisslen, M., Reiss, P. & Portegies, P. HIV-1 infection and cognitive impairment in the cART era: a review. *AIDS* **25**, 561–575 (2011).
- Grant, I. et al. Asymptomatic HIV-associated neurocognitive impairment increases risk for symptomatic decline. *Neurology* **82**, 2055–2062 (2014).
- Nath, A. Human immunodeficiency virus (HIV) proteins in neuropathogenesis of HIV dementia. *J. Inf. Dis.* **186**, S193–S198 (2002).
- Ellis, R., Langford, D. & Masliah, E. HIV and antiretroviral therapy in the brain: neuronal injury and repair. *Nat. Rev. Neurosci.* **8**, 33–44 (2007).
- Sabatier, J. M. et al. Evidence for neurotoxic activity of tat from human immunodeficiency virus type 1. *J. Virol.* **65**, 961–967 (1991).
- Kim, H. J., Martemyanov, K. A. & Thayer, S. A. Human immunodeficiency virus protein Tat induces synapse loss via a reversible process that is distinct from cell death. *J. Neurosci.* **28**, 12604–12613 (2008).
- Nath, A. & Steiner, J. Synaptodendritic injury with HIV-Tat protein: What is the therapeutic target? *Exp. Neurol.* **251**, 112–114 (2014).
- Price, T., Ercal, N., Nakaoka, R. & Banks, W. A. HIV-1 viral proteins gp120 and Tat induce oxidative stress in brain endothelial cells. *Brain Res.* **1045**, 57–63 (2005).
- Banerjee, A., Zhang, X., Manda, K. R., Banks, W. A. & Ercal, N. HIV proteins (gp120 and Tat) and methamphetamine in oxidative stress-induced damage in the brain: potential role of the thiol antioxidant N-acetylcysteine amide. *Free Radic. Biol. Med.* **48**, 1388–1398 (2010).
- Mastrantonio, R. et al. HIV-Tat induces the Nrf2/ARE pathway through NMDA receptor-elicited spermine oxidase activation in human neuroblastoma cells. *PLoS ONE* **11**, e0149802 (2016).
- Agrawal, L., Louboutin, J. P., Reyes, B. A., Van Bockstaele, E. J. & Strayer, D. S. HIV-1 Tat neurotoxicity: a model of acute and chronic exposure, and neuroprotection by gene delivery of antioxidant enzymes. *Neurobiol. Dis.* **45**, 657–670 (2012).
- Trillo-Pazos, G., McFarlane-Abdulla, E., Campbell, I. C., Pilkington, G. J. & Everall, I. P. Recombinant nef HIV-1IIB protein is toxic to human neurons in culture. *Brain Res.* **864**, 315–326 (2000).
- Rivera, J. et al. Infusion of HIV-1 Nef-expressing astrocytes into the rat hippocampus induces enteropathy and interstitial pneumonitis and increases blood-brain-barrier permeability. *PLoS ONE* **14**, <https://doi.org/10.1371/journal.pone.0225760> (2019).
- Chompre, G. et al. Astrocytic expression of HIV-1 Nef impairs spatial and recognition memory. *Neurobiol. Dis.* **49**, 128–136 (2013).
- Lehmann, M. H., Lehmann, J. M. & Erfle, V. Nef-induced CCL2 expression contributes to HIV/SIV brain invasion and neuronal dysfunction. *Front Immunol.* **10**, 2447 (2019).
- Gorwood, J. et al. SIV Infection and the HIV proteins Tat and Nef induce senescence in adipose tissue and human adipose stem cells, resulting in adipocyte dysfunction. *Cells* **9**, <https://doi.org/10.3390/cells9040854> (2020).
- Olivetta, E. et al. HIV-1 Nef regulates the release of superoxide anions from human macrophages. *Biochemical J.* **390**, 591–602 (2005).
- Salmen, S. et al. HIV-1 Nef associates with p22-phox, a component of the NADPH oxidase protein complex. *Cell. Immunol.* **263**, 166–171 (2010).
- Tiede, L. M., Cook, E. A., Morsey, B. & Fox, H. S. Oxygen matters: tissue culture oxygen levels affect mitochondrial function and structure as well as responses to HIV viroproteins. *Cell Death Dis.* **2**, e246 (2011).
- Coyle, J. T. & Puttfarcken, P. Oxidative stress, glutamate, and neurodegenerative disorders. *Science* **262**, 689–695 (1993).
- Halliwel, B. Reactive oxygen species and the central nervous system. *J. Neurochemistry* **59**, 1609–1623 (1992).
- Mollace, V. et al. Oxidative stress and neuroAIDS: triggers, modulators and novel antioxidants. *Trends Neurosci.* **24**, 411–416 (2001).
- Ivanov, A. V. et al. Oxidative stress during HIV infection: mechanisms and consequences. *Oxid. Med. Cell Longev.* **2016**, 8910396 (2016).
- Finkel, T. & Holbrook, N. J. Oxidants, oxidative stress and the biology of ageing. *Nature* **408**, 239–247 (2000).
- Bhat, A. H. et al. Oxidative stress, mitochondrial dysfunction and neurodegenerative diseases; a mechanistic insight. *Biomed. Pharmacother.* **74**, 101–110 (2015).
- Giorgio, M., Trinei, M., Migliaccio, E. & Pelicci, P. G. Hydrogen peroxide: a metabolic by-product or a common mediator of ageing signals? *Nat. Rev. Mol. Cell Biol.* **8**, 722–728 (2007).
- Lopez-Otin, C., Blasco, M. A., Partridge, L., Serrano, M. & Kroemer, G. The hallmarks of aging. *Cell* **153**, 1194–1217 (2013).
- Nguyen, T. P., Soukup, V. M. & Gelman, B. B. Persistent hijacking of brain proteasomes in HIV-associated dementia. *Am. J. Pathol.* **176**, 893–902 (2010).
- Pulliam, L. HIV regulation of amyloid beta production. *J. Neuroimmune Pharm.* **4**, 213–217 (2009).
- Sondermann, H. et al. Structure of a Bag/Hsc70 complex: convergent functional evolution of Hsp70 nucleotide exchange factors. *Science* **291**, 1553–1557 (2001).
- Takayama, S. & Reed, J. C. Molecular chaperone targeting and regulation by BAG family proteins. *Nat. Cell Biol.* **3**, E237–E241 (2001).
- Ganassi, M. et al. A surveillance function of the HSPB8-BAG3-HSP70 chaperone complex ensures stress granule integrity and dynamism. *Mol. Cell* **63**, 796–810 (2016).
- Mateju, D. et al. An aberrant phase transition of stress granules triggered by misfolded protein and prevented by chaperone function. *EMBO J.* **36**, 1669–1687 (2017).
- Minoia, M. et al. BAG3 induces the sequestration of proteasomal clients into cytoplasmic puncta: implications for a proteasome-to-autophagy switch. *Autophagy* **10**, 1603–1621 (2014).
- Townsend, P. A., Cutress, R. I., Sharp, A., Brimmell, M. & Packham, G. BAG-1: a multifunctional regulator of cell growth and survival. *Biochimica et Biophysica Acta (BBA) - Rev. Cancer* **1603**, 83–98 (2003).
- Gamerding, M. et al. Protein quality control during aging involves recruitment of the macroautophagy pathway by BAG3. *EMBO J.* **28**, 889–901 (2009).
- Gamerding, M., Kaya, A. M., Wolfrum, U., Clement, A. M. & Behl, C. BAG3 mediates chaperone-based aggresome-targeting and selective autophagy of misfolded proteins. *EMBO Rep.* **12**, 149–156 (2011).
- Behl, C. Breaking BAG: the co-chaperone BAG3 in health and disease. *Trends Pharm. Sci.* **37**, 672–688 (2016).
- Chakraborty, D. et al. Enhanced autophagic-lysosomal activity and increased BAG3-mediated selective macroautophagy as adaptive response of neuronal cells to chronic oxidative stress. *Redox Biol.* **24**, 101181 (2019).
- Mohseni Ahooyi, T. et al. Perturbation of synapsins homeostasis through HIV-1 Tat-mediated suppression of BAG3 in primary neuronal cells. *Cell Death Dis.* **10**, 473 (2019).
- Whittemore, E. R., Loo, D. T., Watt, J. A. & Cotman, C. W. A detailed analysis of hydrogen peroxide-induced cell-death in primary neuronal culture. *Neuroscience* **67**, 921–932 (1995).
- Ricart, K. C. & Fiszman, M. L. Hydrogen peroxide-induced neurotoxicity in cultured cortical cells grown in serum-free and serum-containing media. *Neurochem. Res.* **26**, 801–808 (2001).
- O'Riordan, S. L. & Lowry, J. P. In vivo characterisation of a catalase-based biosensor for real-time electrochemical monitoring of brain hydrogen peroxide in freely-moving animals. *Anal. Methods* **9**, 1253–1264 (2017).
- Bilan, D. S. & Belousov, V. V. In vivo imaging of hydrogen peroxide with HyPer probes. *Antioxid. Redox Signal* **29**, 569–584 (2018).
- Zhao, S. et al. BAG3 promotes autophagy and glutaminolysis via stabilizing glutaminase. *Cell Death Dis.* **10**, 284 (2019).
- Alberti, S. et al. Ubiquitylation of BAG-1 suggests a novel regulatory mechanism during the sorting of chaperone substrates to the proteasome. *J. Biol. Chem.* **277**, 45920–45927 (2002).
- Takayama, S. et al. Expression and location of Hsp70/Hsc-binding anti-apoptotic protein BAG-1 and its variants in normal tissues and tumor cell lines. *Cancer Res.* **58**, 3116–3131 (1998).
- Yang, X. et al. Human BAG-1/RAP46 protein is generated as four isoforms by alternative translation initiation and overexpressed in cancer cells. *Oncogene* **17**, 981–989 (1998).

55. Klajps, C. L., Jayaraj, G. G. & Hartl, F. U. Pathways of cellular proteostasis in aging and disease. *J. Cell Biol.* **217**, 51–63 (2018).
56. Mattson, M. P. & Magnus, T. Ageing and neuronal vulnerability. *Nat. Rev. Neurosci.* **7**, 278–294 (2006).
57. Grubman, A. et al. A single-cell atlas of entorhinal cortex from individuals with Alzheimer's disease reveals cell-type-specific gene expression regulation. *Nat. Neuro* **22**, 2087–2097 (2019).
58. Gurwitz, K. T. et al. Time-dependent, HIV-Tat-induced perturbation of human neurons in vitro: towards a model for the molecular pathology of HIV-associated neurocognitive disorders. *Front. Mol. Neurosci.* **10**, 163 (2017).
59. Valles, S. L. et al. Function of glia in aging and the brain diseases. *Int. J. Med. Sci.* **16**, 1473–1479 (2019).
60. Malva, J. O., Cunha, R. A., Oliveira, C. R. & Rego, A. C. *Interaction Between Neurons and Glia in Aging and Disease* (Springer, 2007).
61. Salas, I. H., Burgado, J. & Allen, N. J. Glia: victims or villains of the aging brain? *Neurobiol. Dis.* **143**, 105008 (2020).
62. Fields, J. et al. HIV-1 Tat alters neuronal autophagy by modulating autophagosome fusion to the lysosome: implications for HIV-associated neurocognitive disorders. *J. Neurosci.* **35**, 1921–1938 (2015).
63. Campbell, G. R., Rawat, P., Bruckman, R. S. & Spector, S. A. Human immunodeficiency virus type 1 Nef inhibits autophagy through transcription factor EB sequestration. *PLoS Pathog.* **11**, e1005018 (2015).
64. Cornelli, U. Treatment of Alzheimer's disease with a cholinesterase inhibitor combined with antioxidants. *Neurodegener. Dis.* **7**, 193–202 (2010).
65. Kabir, M. T. et al. Combination drug therapy for the management of Alzheimer's disease. *Int. J. Mol. Sci.* **21**, <https://doi.org/10.3390/ijms21093272> (2020).
66. Cao, Y. L. et al. A role of BAG3 in regulating SNCA/alpha-synuclein clearance via selective macroautophagy. *Neurobiol. Aging* **60**, 104–115 (2017).
67. Lei, Z., Brizzee, C. & Johnson, G. V. W. BAG3 facilitates the clearance of endogenous tau in primary neurons. *Neurobiol. Aging* **36**, 241–248 (2015).
68. Carra, S., Seguin, S. J., Lambert, H. & Landry, J. HspB8 chaperone activity toward poly(Q)-containing proteins depends on its association with Bag3, a stimulator of macroautophagy. *J. Biol. Chem.* **283**, 1437–1444 (2008).
69. Kermer, P. et al. BAG1 is neuroprotective in in vivo and in vitro models of Parkinson's disease. *J. Mol. Neuro* **55**, 587–595 (2015).
70. Mohseni Ahooyi, T. et al. Network analysis of hippocampal neurons by microelectrode array in the presence of HIV-1 Tat and cocaine. *J. Cell. Physiol.* **233**, 9299–9311 (2018).
71. Li, T.-S. & Marbán, E. Physiological levels of reactive oxygen species are required to maintain genomic stability in stem cells. *Stem Cells* **28**, 1178–1185 (2010).
72. Luo, L. et al. Effects of antioxidants on the quality and genomic stability of induced pluripotent stem cells. *Sci. Rep.* **4**, 3779 (2014).
73. Heaton, R. K. et al. HIV-associated neurocognitive disorders before and during the era of combination antiretroviral therapy: differences in rates, nature, and predictors. *J. Neurovirol.* **17**, 3–16 (2011).
74. Torkzaban, B. et al. The lncRNA LOC102549805 (U1) modulates neurotoxicity of HIV-1 Tat protein. *Cell Death Dis.* **11**, 835 (2020).